Polarization Self-Screened Multiple Quantum Wells for Deep Ultraviolet Light-Emitting Diodes to Enhance the Optical Power

Chunshuang Chu, Kangkai Tian, Hua Shao, Jiamang Che, Yonghui Zhang, and Zi-Hui Zhang

***Abstract*—We experimentally and numerically propose a deep ultraviolet light-emitting diode (DUV LED) possessing the quantum barriers (QBs) with the gradually reduced Al composition along the [0001] orientation. The induced negative polarization bulk charges in the graded QBs can screen the positive polarization sheet charges at the QB/quantum well (QW) interface, i.e., generating the polarization self-screening effect, which weakens the electric field in the QWs. The polarization self-screened feature is important in enhancing the overlap level of the electron and hole wave functions within the active region and increasing the hole injection, thus improving the electroluminescence intensity and the optical power.**

***Index Terms*—DUV LED, polarization self-screening effect, polarization bulk charge, hole injection.**

I. Introduction

RECENTLY, AlGaN-based deep ultraviolet light-emitting diodes (DUV LEDs) have attracted extensive research attention due to the promising application prospects in water sterilization, air purification, ultraviolet curing, biological medication, light communication etc., especially in the case of the global spread of the Corona Virus Disease from the year of 2019 till now (i.e., COVID-19) [1]. However, at the current stage, it is difficult to make high external quantum efficiency (EQE) for DUV LEDs as the emission wavelength decreases because of the poor crystalline-quality epilayers, low carrier injections, current crowding effect and the strong polarization effect, ect. [2]. Among them, the polarization effect is the intrinsic characteristic for III-nitride material with crystal asymmetry, which shows the significant impact on both the carrier transport and radiative recombination processes in the AlGaN/AlGaN multiple quantum wells (MQWs) grown along the [0001] orientation [3]. On one hand, the polarization electric field within the MQWs will cause the tilted energy band and finally lead to a spatial separation of electron-hole wave functions in the quantum well, which is known as the quantum-confined Stark effect (QCSE) [4]. On the other hand, the tilted energy band in the active region will increase the electron leakage into the p-type hole injection layer, which may recombine with holes in the p-region and further suppress the hole injection capability [5]. Proposals to suppress the QCSE in the active region include using the non-polar and semipolar substrate [6], [7] and utilizing the AlInGaN/AlInGaN MQW region [8], [9]. However, the above methods have strict requirements for epitaxial growth technology. Therefore, a variety of device structural designs are proposed to modulate the polarization charge density and polarization field intensity at the AlGaN/AlGaN quantum well (QW)/quantum barrier (QB) interface to suppress the QCSE. For example, the QWs with the graded Al composition [10], the staggered QWs [11] and the very thin QWs [12] are designed to enhance the overlap level of electron-hole wave functions for DUV LEDs. Moreover, the use of the Si-doped AlGaN QBs for DUV LEDs is also a relatively simple way to screen the polarization field in the active region, which reduces the polarization electric field intensity in the QWs to 2×10^5 V/cm [13]. However, it can be further found that the use of the Si-doped QBs will block the hole injection efficiency into the MQWs. The essence of QCSE suppression by using Si-doped quantum barriers is that the ionized immobile charges can screen the polarization interface charges in the active region. Therefore, the alternative immobile charged particles have to be proposed. Zhang *et al.* have ever proposed the polarization self-screening effect for GaN-based blue and UV LEDs [14], [15], such that they grade the InN composition in the quantum barriers so that the polarization induced bulk charges can be produced [16], and this immobile polarization bulk charges can screen the polarization interface charges, thus decreasing the polarization induced electric field in the quantum wells. However, although the polarization self-screened design can suppress the QCSE, the optical power for GaN-based UV LED is not enhanced due to the reduced conduction band barrier height and the stronger electron

Manuscript received July 20, 2021; revised September 2, 2021; accepted September 21, 2021. Date of publication September 24, 2021; date of current version October 11, 2021. This work was supported in part by the National Natural Science Foundation of China under Grant 62074050, in part by the Natural Science Foundation of Hebei Province under Grants F2020202030 and F2018202080, in part by the research fund by the State Key Laboratory of Reliability and Intelligence of Electrical Equipment, Hebei University of Technology under Grant EERI_PI2020008, and in part by the Research Fund by Jiangsu Provincial Key Laboratory of Photonic and Electronic Materials Sciences and Technology, Nanjing University under Grant njuzds2021-005. *(Chunshuang Chu and Kangkai Tian contributed equally to this work.) (Corresponding author: Zi-Hui Zhang.)*

The authors are with the Key Laboratory of Electronic Materials and Devices of Tianjin, School of Electronics and Information Engineering, Hebei University of Technology, Tianjin 300401, China, and also with the State Key Laboratory of Reliability and Intelligence of Electrical Equipment, Hebei University of Technology, Tianjin 300401, China (e-mail: chuchunshuang@hotmail.com; tiankangkai24@hotmail.com; shaohua0501@hotmail.com; jiamang_che@hotmail.com; zhangyh@hebut.edu.cn; zh.zhang@hebut.edu.cn).

Digital Object Identifier 10.1109/JPHOT.2021.3115341

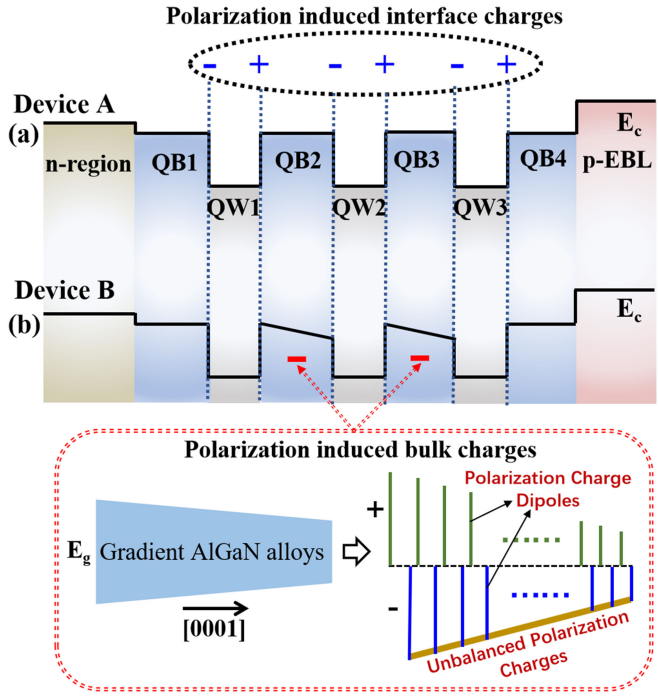

Fig. 1. Conduction band diagrams and charge profiles for (a) Device A and (b) Device B, respectively. The inset figure shows the generation mechanism of the polarization induced bulk charges.

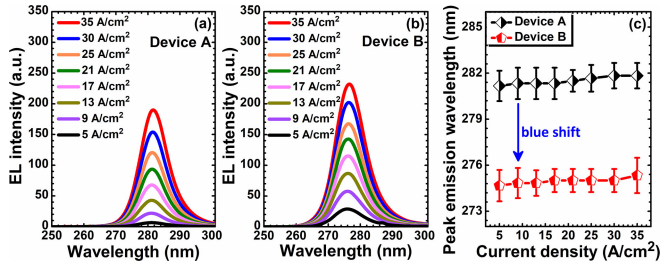

Fig. 2. Measured EL spectra for (a) Device A and (b) Device B in terms of different injection current density levels, and (c) measured peak emission wavelengths in terms of different injection current density levels for Device A and Device B, respectively.

leakage level [15]. Therefore, it is worth investigating whether such polarization self-screened active region can help to increase the optical power for AlGaN-based DUV LEDs with unique valence band profiles for heavy hole (HH), light hole (LH) and crystal-field split-off hole (CH) [17], which, besides the QCSE in the active region, have the even lower hole concentration in the p-type region.

II. Device Architectures

To investigate the impact of the polarization self-screening effect for the proposed device on the electron-hole recombination and the carrier transport processes, two DUV LEDs (i.e., Device A and Device B) are grown on the [0001]-orientated sapphire substrate in the metal organic chemical vapor deposition (MOCVD) technology and the calculated models are shown in Figs. 1(a) and 1(b). The studied two DUV LEDs possess a 4 μm thick n-$Al_{0.60}Ga_{0.40}N$ layer (n-doping $= 5 \times 10^{18}$ cm^{-3}) as the electron injection layer (i.e., n-region). The MQW region is composed of 3-pair 3 nm thick $Al_{0.45}Ga_{0.55}N$/10 nm thick $Al_xGa_{1-x}N$ MQW stacks. The structures of Devices A and B differ only in the $Al_xGa_{1-x}N$ QBs. For Device A, the constant Al composition x of four $Al_xGa_{1-x}N$ QBs is set to 58%. For Device B, the Al composition linearly decreases along the [0001] orientation from 58% to 53% for the two QBs in the middle of the MQW region, while the Al composition in the other two QBs is 58%. The negative polarization-induced bulk charge density in the two middle QBs for Device B is $\sim$1.44 $\times 10^{18}$ cm^{-3}. Then, a 10 nm thick p-$Al_{0.60}Ga_{0.40}N$ EBL, a 50 nm thick p-$Al_{0.40}Ga_{0.60}N$ layer and a 50 nm thick p-GaN layer are successively capped on top of the MQW region. According to the high activation energy of Mg dopant [18], [19], the hole concentration for the p-type layers is $\sim 3 \times 10^{17}$ cm^{-3}.

Then, the standard chip fabrications are implemented by using the photolithography, the inductively coupled plasma etch (ICP), the electron beam evaporation and the rapid thermal annealing (RTA) technology after the epitaxial growth. For Devices A and B, the 20 nm/60 nm/30 nm/100 nm thick Ti/Al/Ti/Au metal stack layer is deposited on the exposed n-$Al_{0.60}Ga_{0.40}N$ electron injection layer as the n-electrode. Next, the 10 nm/10 nm thick Ni/Au current spreading layer is deposited on the p-GaN layer as the p-contact. The n-type and p-type Ohmic contact are respectively achieved by annealing in the nitrogen ambient for 60 seconds at 650 °C and in the oxygen atmosphere for 3 minutes at 450 °C. Finally, the 800 nm/20 nm/100 nm thick Al/Ti/Au metal stack layer is deposited on the current spreading layer as the reflective p-electrode. After the device fabrication, the calibrated integrating sphere is used to measure the electroluminescence (EL) spectra from bottom of Device A and Device B chips.

In addition, the device physics for Devices A and B are further discussed by using APSYS software, which is able to calculate the overlap level of electron-hole wave functions, the electric field profiles, and the energy band, etc. [20]. In the calculation models, the energy band offset ratio is assumed to be 50/50 for AlGaN/AlGaN material systems [21]. The values of Auger recombination coefficient and the Shockley-Read-Hall (SRH) recombination lifetime are 1.0×10^{-30} cm^6/s and 10 ns, respectively [20], [22]. The spontaneous and piezoelectric polarization effects at each lattice-mismatched heterojunction have been taken into account. However, considering the strain relaxation by generating dislocations, a 40% polarization level is assumed, such that the other 60% of the theoretical polarization chargers are not considered [23]. The bulk polarization charge density that is used for the $Al_xGa_{1-x}N$ QBs with the graded Al composition has also been considered [14]. Besides, other important parameters of semiconductors used in this calculated model can be found elsewhere [24].

III. Results and Discussion

Firstly, we show the measured electroluminescence (EL) spectra in terms of different injection current density levels for Device A and Device B in Figs. 2(a) and (b), respectively.

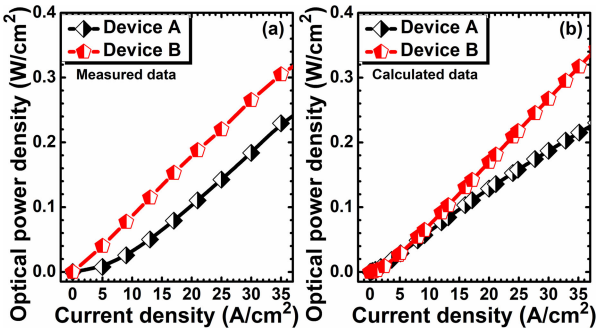

Fig. 3. (a) Experimentally measured and (b) numerically calculated optical power density in terms of the current injection density for Device A and Device B, respectively.

It is obvious that the EL intensity for Device A and Device B increases as the current density increases from 5 A/cm^2 to 35 A/cm^2. In addition, the emission intensity for Device B is significantly stronger than that for Device A at the same current, which indicates that the QBs with the graded Al composition are helpful to improve the performance for DUV LEDs. Fig. 2(c) further summarizes the peak emission wavelengths in terms of different injection current density levels for Device A and Device B. It can be found that the peak emission wavelengths for Device B are all shorter than that for Device A and the blueshift is up to ~6 nm for Device B, which indirectly shows that the polarization electric field in the QW for Device B is mitigated, thus significantly suppressing the QCSE.

Figs. 3(a) and (b) present the experimentally measured and calculated optical power for Device A and Device B, respectively. The calculated optical power has the same trendline with the measured optical power, i.e., the optical power for Device B is higher than that for Device A both numerically and experimentally. It can be seen that the optical power for DUV LEDs can be greatly enhanced when the polarization self-screening active region is utilized. In order to further analyze the effect of such design on the performance for DUV LEDs, it is necessary to investigate the electric field profiles, the energy band distribution, the carrier distribution and the radiative recombination rate in the active region, which will be discussed in an in-depth level subsequently.

Fig. 4(a) shows the electric field distribution profiles in the active region for Devices A and B at the injection current density of 25 A/cm^2. It can be seen that the electric field intensity in the QBs and QWs for Device B is significantly lower than that for Device A. This is mainly because the negative bulk polarization charges of ~1.44×10^{18} cm^{-3} can be generated in the QBs when the Al composition of the QBs linearly decreases, which can effectively screen the positive interface polarization charges at the interface of the QBs and the QWs. According to the formula $\int_0^{L_b} E_b dx = E_w \times L_w$, we can find that E_w is closely related to E_b, L_b and L_w [17]. Here, E_b and E_w represent the electric field intensity in the QBs and the QWs, respectively; L_b and L_w represent the thickness of the QBs and the QWs, respectively. Therefore, as the electric field intensity of the QBs decreases, the electric field in the QWs for Device B gradually decreases.

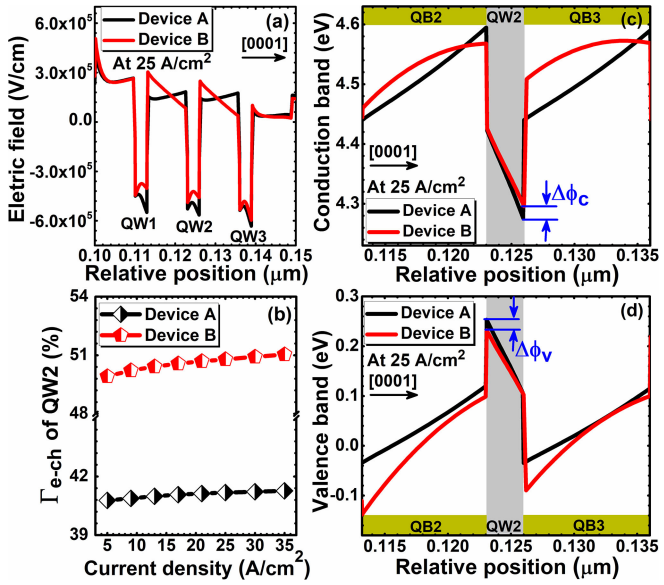

Fig. 4. (a) Calculated electric field profiles for Devices A and B at the injection current density of 25 A/cm^2, (b) spatial overlap levels ($\Gamma_{e\text{-}ch}$) of electron wave functions and the crystal-field split-off hole wave functions in QW2 for Devices A and B, (c) conduction band profiles and (d) valence band profiles for Device A and Device B at the injection current density of 25 A/cm^2.

As shown in Fig. 4(b), we further investigate the overlap level ($\Gamma_{e\text{-}ch}$) of the electron wave function in the conduction band and hole wave function in the CH band of the intermediate quantum well (QW2) for Devices A and B. It can be seen that the $\Gamma_{e\text{-}ch}$ for Device B is significantly higher than that for Device A, which once again proves that the QCSE in Device B can be effectively suppressed. In addition, with the increase of injection current, the $\Gamma_{e\text{-}ch}$ for Devices A and B tends to slightly increase, which is because the excessive carrier injection can effectively screen the interface polarization charge at the interface of the QW2, leading to the further reduction for the polarization electric field in the QW2. Moreover, by comparing the conduction band and the valence band for Devices A and B in Figs. 4(c) and (d), we can find that the energy band distribution for Device B tends to be flattened due to the decrease of the polarization electric field. The calculation results show that, for Device B, the conduction band and valence band respectively move up and down (i.e., $\Delta\phi_c$ and $\Delta\phi_v$) by ~20 meV, respectively, which explains the observations in Fig. 4(b), such that the carrier wave functions in the QW for Device B has a larger overlap level.

As shown in Figs. 5(a), (b) and (c), we show the hole concentration, the electron concentration and the radiative recombination rate profiles in the MQW region for Devices A and B at the injection current density of 25 A/cm^2, respectively. From Fig. 5(a), we can see that the hole concentration in the active region for Device B is significantly higher than that for Device A. This is mainly because that the reduced valence band barrier height of the QBs promotes the hole injection into the active region when the average Al composition of the QBs decreases for Device B. However, the QBs with the graded Al composition will also reduce the conduction band barrier height, which will weaken the electrons confinement ability of the QWs and cause

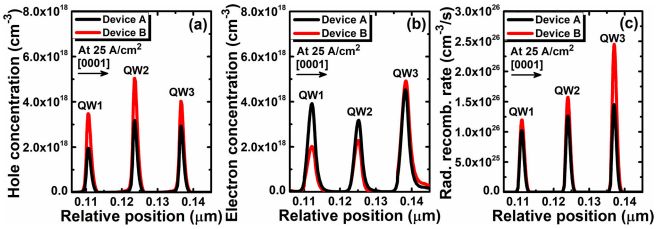

Fig. 5. (a) Hole concentration profiles, (b) electron concentration profiles and (c) radiative recombination rate profiles in the MQW region for Device A and Device B, respectively. Data are calculated at the injection current density of 25 A/cm^2.

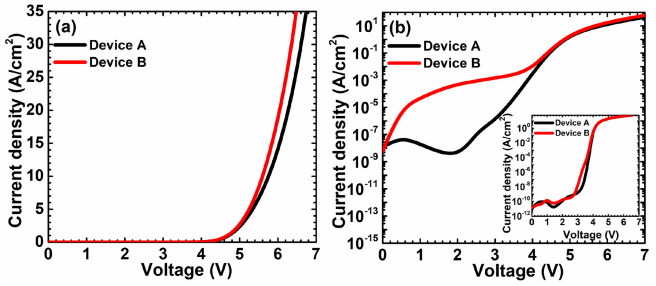

Fig. 6. Measured the current-voltage characteristic curves in (a) linear scale and (b) semi-log scale for Devices A and B. The inset in Figure (b) shows the calculated current-voltage characteristic curves in semi-log scale for Devices A and B.

more electrons to be transported to the QW near the p-EBL side. Therefore, Fig. 5(b) shows the poor electron concentration in the first two QWs for Device B. Nevertheless, as shown in Fig. 5(c), the radiative recombination rate for Device B is higher than that for Device A in all the quantum wells, and this is due to the increased hole injection efficiency and the decreased QCSE in the QW. Thus the optical power and EL intensity can be increased significantly [see Figs. 2 and 3].

Lastly, we present the current-voltage (I-V) characteristics which are measured by Keithley 2400 for Devices A and B in Fig. 6(a). We can find that Device B possesses the reduced forward voltage, which is attributed to the better hole injection efficiency. The specific resistance for the two devices are 0.030 and 0.028 Ω·cm^2 for Devices A and B, respectively. Moreover, it can be also seen that the measured leakage current is increased before the devices reach the turn-on voltage as presented in Fig. 6(b). The increased leakage current can be caused by the reduced conduction band barrier height for Device B with the graded quantum barriers. The inset of Fig. 6(b) shows the numerically calculated I-V characteristics and the conclusion is consistent with measured results in Fig. 6(b), such that we observe more leakage current for Device B before the devices are turned on.

IV. Conclusion

To conclude, we have demonstrated two DUV LEDs that have different quantum barriers. The impact of the different quantum barriers on the carrier injection and the overlap level for the electron-hole wave functions has been studied. By gradually decreasing the Al composition along the [0001] direction within the quantum barriers, the negative bulk polarization charges can be formed, which can effectively screen the positive interface polarization charges at the interface of the quantum barriers and the quantum wells, thereby alleviating the QCSE. Thus, the energy band becomes flattened in the quantum well for the proposed device, which is beneficial to increase the overlap rate of electron-CH wave functions and results in the blueshift of the peak wavelength. Moreover, the valence band barrier heights of the quantum barriers are reduced because of the decreased average Al composition of the quantum barriers, which enhances the hole injection efficiency. As a result, the radiative recombination rate, the optical power and EL intensity are significantly enhanced for the proposed DUV LED with polarization self-screening effect in the MQWs. We strongly believe the proposed structure is promising to develop the high-efficiency DUV LEDs. The findings here also provide additional physical understanding for AlGaN-based DUV LEDs.

References

[1] H. Amano, R. Collazo, C. D. Santi, and S. Einfeldt, "The 2020 UV emitter roadmap," *J. Phys. D-Appl. Phys.*, vol. 53, no. 50, Dec. 2020, Art. no. 503001, doi: 10.1088/1361-6463/aba64c.

[2] J. Park, J. K. Kim, J. Cho, and T. Seong, "Group III nitride based ultraviolet light-emitting diodes ways: Ways of increasing external quantum efficiency," *ECS J. Solid State Sci. Technol.*, vol. 6, no. 4, pp. Q42–Q52, Feb. 2017, doi: 10.1149/2.0111704jss.

[3] E. F. Schubert, *Light Emitting Diodes*, 2nd ed. New York, NY, USA: Cambridge Univ. Press, 2006.

[4] U. T. Schwarz, H. Braun, K. Kojima, Y. Kawakami, S. Nagahama, and T. Mukai, "Interplay of built-in potential and piezoelectric field on carrier recombination in green light emitting InGaN quantum wells," *Appl. Phys. Lett.*, vol. 91, no. 12, Sep. 2007, Art. no. 123503, doi: 10.1063/1.2786602.

[5] J. Cho, E. F. Schubert, and J. K. Kim, "Efficiency droop in LEDs-challenges and countermeasures," *Laser Photon. Rev.,* vol. 7, no. 3, pp. 408–421, May 2013, doi: 10.1002/lpor.201200025.

[6] Y. Ji *et al.*, "Comparative study of field-dependent carrier dynamics and emission kinetics of InGaN/GaN light-emitting diodes grown on (11-22) semipolar versus (0001) polar planes," *Appl. Phys. Lett.*, vol. 104, no. 14, Apr. 2014, Art. no. 143506, doi: 10.1063/1.4870840.

[7] M. Jo, Y. Itokazu, S. Kuwaba, and H. Hirayama, "Improved crystal quality of semipolar AlN by employing a thermal annealing technique with MOVPE," *J. Cryst Growth*, vol. 507, pp. 307–309, Feb. 2019, doi: 10.1016/j.jcrysgro.2018.11.009.l.

[8] J. C. Zhang, Y. H. Zhu, T. Egawa, S. Sumiya, M. Miyoshi, and M. Tanaka, "Quantum-well and localized state emissions in AlInGaN deep ultraviolet light-emitting diodes," *Appl. Phys. Lett.*, vol. 91, no. 22, Nov. 2007, Art. no. 221906, doi: 10.1063/1.2817947.

[9] Z. Wu, X. Zhang, T. Liang, Z. C. Feng, and Y. Cui, "Effects of growth temperature on characteristics of Mg-delta-doped p-AlInGaN epi-layers," *Superlattice Microst,* vol. 98, pp. 181–186, Aug. 2016, doi: 10.1016/j.spmi.2016.08.025.

[10] H. Yu *et al.*, "Enhanced performance of an AlGaN-based deep-ultraviolet LED having graded quantum well structure," *IEEE Photon. J.*, vol. 11, no. 4, Aug. 2019, Art. no. 8201006, doi: 10.1109/JPHOT.2019.2922280.

[11] M. Zhang *et al.*, "Performance improvement of AlGaN-based deep ultraviolet light-emitting diodes by using staggered quantum wells," *Superlattice Microst.,* vol. 75, pp. 63–71, Jul. 2014, doi: 10.1016/j.spmi.2014.07.002.

[12] K. Tian *et al.*, "Interplay between various active regions and the interband transition for AlGaN-based deep-ultraviolet light-emitting diodes to enable a reduced TM-polarized emission," *J. Appl. Phys.*, vol. 126, no. 24, Dec. 2019, Art. no. 245702, doi: 10.1063/1.5127916.

[13] K. Tian *et al.*, "Investigations on AlGaN-based deep-ultraviolet light-emitting diodes with Si-doped quantum barriers of different doping concentrations," *Phys Status Solidi-R*, vol. 12, no. 1, Jan. 2018, Art. no. 1700346, doi: 10.1002/pssr.201700346.

[14] Z.-H. Zhang *et al.*, "Self-screening of the quantum confined stark effect by the polarization induced bulk charges in the quantum barriers," *Appl. Phys. Lett.*, vol. 104, no. 24, Jun. 2014, Art. no. 243501, 10.1063/1.4883894.

[15] K. Tian *et al.*, "On the polarization self-screening effect in multiple quantum wells for nitride-based near ultraviolet light-emitting diodes," *Chin. Opt. Lett.*, vol. 17, no. 12, Dec. 2019, Art. no. 122301, doi: 10.3788/COL201917.122301.

[16] J. Simon, V. Protasenko, C. Lian, H. L. Xing, and D. Jena, "Polarization-induced hole doping in wide–band-gap uniaxial semiconductor heterostructures," *Science*, vol. 327, no. 5961, pp. 60–64, Jan. 2010, doi: 10.1126/science.1183226.

[17] K. B. Nam, J. Li, M. L. Nakarmi, J. Y. Lin, and H. X. Jiang, "Unique optical properties of AlGaN alloys and related ultraviolet emitters," *Appl. Phys. Lett.*, vol. 84, no. 25, pp. 5264–5266, Jun. 2004, doi: 10.1063/1.1765208.

[18] I. P. Smorchkova *et al.*, "Mg doping of GaN layers grown by plasma-assisted molecular-beam epitaxy," *Appl. Phys. Lett.*, vol. 76, no. 6, pp. 718–720, Dec. 2000, doi: 10.1063/1.125872.

[19] Y.-H. Liang and E. Towe, "Progress in efficient doping of high aluminum-containing group III-nitrides," *Appl. Phys. Rev.*, vol. 5, no. 1, Mar. 2018, Art. no. 011107, doi: 10.1063/1.5009349.

[20] Y.-K. Kuo, J.-Y. Chang, F.-M. Chen, Y.-H. Shih, and H.-T. Chang, "Numerical investigation on the carrier transport characteristics of AlGaN deep-UV light-emitting diodes," *IEEE J. Quantum Elect.*, vol. 52, no. 4, Apr. 2016, Art. no. 3300105, doi: 10.1109/JQE.2016.2535252.

[21] J. Piprek, "Efficiency droop in nitride-based light-emitting diodes," *Phys. Status Solidi A*, vol. 207, no. 10, pp. 2217–2225, Jul. 2010, doi: 10.1002/pssa.201026149.

[22] F. Nippert *et al.*, "Auger recombination in AlGaN quantum wells for UV light-emitting diodes," *Appl. Phys. Lett.*, vol. 113, no. 7, Aug. 2018, Art. no. 071107, doi: 10.1063/1.5044383.

[23] V. Fiorentini, F. Bernardini, F. D. Sala, A. D. Carlo, and P. Lugli, "Effects of macroscopic polarization in III-V nitride multiple quantum wells," *Phys. Rev. B, Condens. Matter*, vol. 60, no. 12, pp. 8849–8858, Sep. 2002.

[24] I. Vurgaftman and J. R. Meyer, "Band parameters for nitrogen-containing semiconductors," *J. Appl. Phys.*, vol. 94, no. 6, pp. 3675–3696, Jun. 2003, doi: 10.1063/1.1600519.